Novel Trigonal $ZrWMoO_8$ Structure and Its Transformations

Xuebin Deng,[†] Juzhou Tao,*[,‡,§] Xiaojing Yang,[†] Hui Ma,[△] James W. Richardson, Jr.,[‡] and Xinhua Zhao*[,†]

College of Chemistry and Analysis and Test Center, Beijing Normal University, Beijing 100875, P.R. China, Intense Pulsed Neutron Source, Argonne National Laboratory, Argonne, Illinois 43009, and Experiment Physics Center, Institute of High Energy Physics, Chinese Academy of Sciences, Beijing, 100049, P.R. China

Received June 16, 2007. Revised Manuscript Received December 20, 2007

We found two new trigonal polymorphs of cubic $ZrWMoO_8$ with a negative thermal expansion property and successfully solved and refined their structures using X-ray and/or neutron powder diffraction data. The space group of low temperature trigonal $ZrWMoO_8$ is $R\bar{3}$ with cell parameters $a = 9.8722(1)$ Å and $c = 17.5455(2)$ Å, a polytype of the layered trigonal $ZrMo_2O_8$ structure. The space group of high temperature trigonal $ZrWMoO_8$ is $P\bar{3}m1$, and the cell parameters are $a = 5.8404(1)$ Å and $c = 6.0671(2)$ Å. The thermal expansion and phase transition properties of the trigonal and cubic phases were also studied, and consistent structure–property correlation in this system was found. The phase transitions between two forms of trigonal phases and between high temperature trigonal and cubic phases are reversible first order phase transitions. Utilizing the established polymorphous phase transitions, tailorable synthesis of solid oxide materials with controllable thermal expansion property is anticipated in this family.

Introduction

The cubic AM_2O_8 family of solid oxides (A = Zr, Hf and M = Mo, W) has received considerable research attention during the past decade for their large isotropic negative thermal expansion (NTE) over a wide temperature range.[1–3] While controversy still remains over the exact structural mechanism leading to NTE,[4–7] there is consensus that the isotropic NTE property originates from the unique cubic crystal structure.[3] Many groups have been studying isomorphism and polymorphism behaviors of this family,[8–12] both to investigate the crystal structure and thermal property relationship in depth and to explore procedures for tailored synthesis of materials with adjustable thermal expansion properties. The results showed that different AM_2O_8 isomorphous modifications vary significantly in thermal stability, for example, metastable cubic ZrW_2O_8 decomposes into WO_3 and ZrO_2 above 773 °C,[12] while cubic $ZrMo_2O_8$ transforms into a trigonal polymorphous phase over 390 °C instead.[2] By means of Mo atoms partially substituting W atoms, pure phase isomorphous solid solutions $ZrW_{2-x}Mo_xO_8$ were synthesized successfully, through which we are able to modify and control the thermal properties and extend the thermal stability range of cubic ZrW_2O_8 type materials.[12]

In the AM_2O_8 (A = Zr, Hf; M = W, Mo) family of compounds, triclinic,[13] monoclinic,[13–15] orthorhombic,[16–18] trigonal,[19–22] hexagonal,[10] and cubic[2,3] structure types have all been reported. Among them the two trigonal phases α-$ZrMo_2O_8$ and α′-$ZrMo_2O_8$ are most relevant to this work, and the low temperature superstructure α-$ZrMo_2O_8$ phase undergoes a displacive phase transition at 214 °C to a high temperature α′-$ZrMo_2O_8$ phase.[22] There have been structural studies of the $A_{1-x}A_x'M_{2-y}M_y'O_8$ (A = Zr, Hf; M = W, Mo)

* Corresponding author. Fax: +86-10-5880-2075. E-mail: xinhuaz@bnu.edu.cn.
† College of Chemistry, Beijing Normal University.
‡ Argonne National Laboratory.
§ Chinese Academy of Sciences.
△ Analysis and Test Center, Beijing Normal University.

(1) Mary, T. A.; Evans, J. S. O.; Vogt, T.; Sleight, A. W. *Science* **1996**, *272*, 90.
(2) Lind, C.; Wilkinson, A. P.; Hu, Z.; Short, S.; Jorgensen, J. D. *Chem. Mater.* **1998**, *10*, 2335.
(3) Evans, J. S. O.; Mary, T. A.; Vogt, T.; Subramanian, M. A.; Sleight, A. W. *Chem. Mater.* **1996**, *8*, 2809.
(4) Pryde, A. K. A.; Hammonds, K. D.; Dove, M. T.; Heine, V.; Gale, J. D.; Warren, M. C. *J. Phys.: Condens. Matter* **1996**, *8*, 10973.
(5) Cao, D.; Bridges, F.; Kowach, G. R.; Ramirez, A. P. *Phys. Rev. B* **2003**, *68*, 014303-1.
(6) Tucker, M. G.; Goodwin, A. L.; Dove, M. T.; Keen, D. A.; Wells, S. A.; Evans, J. S. O. *Phys. Rev. Lett.* **2005**, *95*, 255501-1.
(7) Tao, J. Z.; Sleight, A. W. *J. Solid State Chem.* **2003**, *173*, 442.
(8) Lind, C.; Wilkinson, A. P.; Rawn, C. J.; Payzant, E. A. *J. Mater. Chem.* **2002**, *12*, 990.
(9) Closmann, C.; Sleight, A. W.; Haygarth, J. C. *J. Solid State Chem.* **1998**, *139*, 424.
(10) Grzechnik, A.; Crichton, W. A.; Syassen, K.; Adler, P.; Mezouar, M. *Chem. Mater.* **2001**, *13*, 4255.
(11) Deng, X.-B.; Zhao, X.-H.; Han, J.-S. *Wuji Huaxue Xuebao* **2005**, *21*, 1357.
(12) Huang, L.; Xiao, Q.-g.; Ma, H.; Li, G.-b.; Liao, F.-h.; Qi, C.-m.; Zhao, X.-h. *Eur. J. Inorg. Chem.* **2005**, 4521.
(13) Carlson, S.; Andersen, A. M. K. *Phys. Rev. B* **2000**, *61*, 11209.
(14) Auray, M.; Quarton, M.; Tarte, P. *Powder Diffr.* **1989**, *4*, 29.
(15) Achary, S. N.; Mukherjee, G. D.; Tyagi, A. K.; Godwal, B. K. *Phys. Rev. B* **2002**, *66*, 184106-1.
(16) Evans, J. S. O.; Hu, Z.; Jorgensen, J. D.; Argyriou, D. N.; Short, S.; Sleight, A. W. *Science* **1997**, *275*, 61.
(17) Jorgensen, J. D.; Hu, Z.; Short, S.; Sleight, A. W.; Evans, J. S. O. *J. Appl. Phys.* **2001**, *89*, 3184.
(18) Allen, S.; Warmingham, N. R.; Gover, R. K. B.; Evans, J. S. O. *Chem. Mater.* **2003**, *15*, 3406.
(19) Auray, M.; Quarton, M.; Tarte, P. *Acta Crystallogr., Sect. C* **1986**, *42*, 257.
(20) Wilkinson, A. P.; Lind, C.; Pattanaik, S. *Chem. Mater.* **1999**, *11*, 101.
(21) Noailles, L. D.; Peng, H. H.; Starkovich, J.; Dunn, B. *Chem. Mater.* **2004**, *16*, 1252.
(22) Allen, S.; Ward, R. J.; Hampson, M. R.; Gover, R. K. B.; Evans, J. S. O. *Acta Crystallogr., Sect. B* **2004**, *60*, 32.

10.1021/cm071605y CCC: $40.75 © 2008 American Chemical Society
Published on Web 01/31/2008

system, [9,12,23,24] especially the $ZrWMoO_8$ solid solution, where only cubic and orthorhombic phases were reported.[12,23]

In the present work, by means of the solid-state route, two trigonal crystal structures of $ZrWMoO_8$, one in low temperature (LTT hereafter) and another in high temperature (HTT hereafter) were obtained. The LTT-$ZrWMoO_8$ is a novel structural type. The phase transformations among these two polymorphous and the cubic structures are also discussed in detail.

Experimental Section

Sample Preparation. Analytical reagent purity $ZrO(NO_3)_2 \cdot 2H_2O$ (Beijing Chemical Reagents Company), $(NH_4)_6W_7O_{24} \cdot 6H_2O$, and $(NH_4)_6Mo_7O_{24} \cdot 4H_2O$ (Tianjin Guangfu Fine Chemical Research Institute) were used as starting materials without further purification. The H_2O content in hydrates was checked and calibrated by a gravimetric method. White precipitation was first obtained by adding 40 mL of an aqueous solution of 0.5 mol·L^{-1} Zr^{4+} and [0.5 + 0.5 mol·L^{-1}] mixed ionic solution [W^{6+} + Mo^{6+}] simultaneously into 30 mL of distilled water dropwise, the mixture was then stirred continuously for 2 h and dried together with the mother liquid to produce a yellowish or white solid. After grinding, this solid product was pressed into pellets, sintered at 600 °C for 5 h, and quenched to room temperature to obtain LTT-$ZrWMoO_8$ samples. As there was no notable weight loss during the heating process, this procedure ensures stoichiometry of the final product. The LTT-$ZrWMoO_8$ sample was pressed into 10 mm pellets under a pressure of 10 MPa and was put into a platinum crucible which was put in a ceramic crucible. The pellet was sintered at 980 °C for 1 h and then quenched to room temperature to produce a cubic $ZrWMoO_8$ phase. HTT-$ZrWMoO_8$ was obtained in situ by heating cubic $ZrWMoO_8$ or LTT-$ZrWMoO_8$ at a certain temperature.

Measurements. Both differential scan calorimetry (DSC) and X-ray diffraction (XRD) measurements were carried out at standard settings described elsewhere.[12] In brief, the DSC measurements were performed in air atmosphere, at the heating rate 5 °C·min^{-1} in the temperature range of 30–400 and 10 °C·min^{-1} in the temperature range of 30–1100 °C.

Room temperature XRD data from 2θ = 10 to 120° and in situ variable temperature XRD data from 2θ =10 to 80° were collected with a step size of 0.0167° (2θ) and step time of 20 s. For collecting in situ variable temperature XRD data, the temperature ramp rate was 30 °C·min^{-1} and waiting time was 3 min before every measurement below 750 °C. Above the temperature, the temperature ramp was 60 °C·min^{-1}, and the data were recorded without waiting time. Room temperature time-of-flight neutron powder diffraction (NPD) data were collected on the General Purpose Powder Diffractometer (GPPD) at the Intense Pulsed Neutron Source, Argonne National Laboratory, with 8 g of LTT-$ZrWMoO_8$ sample over a period of 3 h. The XRD patterns of HTT- and LTT-$ZrWMoO_8$ phases were indexed using the PowderX software suite.[25] Cell parameters at different temperatures were calculated from in situ variable temperature XRD data with both PowderX and Unitcell softwares.[26]

The Q400EM (TA Instruments) thermomechanical analyzer (TMA) with a macro-expansion quartz probe was used to collect the thermal expansion data of cubic $ZrWMoO_8$ ceramic pellets. The data were collected with a heating rate of 5 °C·min^{-1} from room temperature to 750 °C, held for 5 min, and then cooled to room temperature at the same rate under air atmosphere and a constant force of 0.5 N. The cell constant of the instrument was calibrated using aluminum and the temperature was calibrated using the metals In, Sn, Bi, Zn, and Al, as standard substances, respectively.

The density of LTT-$ZrWMoO_8$ powder was measured by a pycnometric method at 30 °C. Prior to the measurement, the pycnometric density of the paraffin oil which acted as an immersion liquid was calibrated using distilled water as the standard at the same temperature.

Refinement of Trigonal $ZrWMoO_8$ Crystal Structures. The GSAS suite [27,28] was used for the structure analysis and refinement. For HTT-$ZrWMoO_8$ only isotropic atomic displacement parameters were refined, whereas for LTT-$ZrWMoO_8$ full anisotropic atomic displacement parameters were refined successfully. The distortion parameters in metal–oxygen coordination polyhedra were calculated with the VICS-II program.[29]

The HTT-$ZrWMoO_8$ structure was refined with X-ray data using the crystal structure of α′-$ZrMo_2O_8$ (space group $P\bar{3}ml$)[22] as the starting model. The LTT-$ZrWMoO_8$ structure was refined with neutron data from the highest resolution detector banks based on the structure model described below. For the refinement of the LTT-$ZrWMoO_8$ structure, before the refinement of the structural parameters, the overall parameters were refined first. The atomic displacement parameters were refined first with the isotropic parameters and then the anisotropic parameters. During final cycle of refinement, a total of 61 parameters were refined (four background parameters, one scale factor, three peak shape parameters, one absorption/reflectivity correction, two cell parameters, 16 fractional atomic coordinates, and 34 anisotropic atomic displacement parameters). To confirm the refinement results, the XRD data were refined using the fixed structural parameters and cell parameters which result from the neutron refinement. For final cycle of XRD refinement, a total of 18 parameters were refined (10 background parameters, one scale factor, five peak shape parameters, one zero offset correction, and one preferred orientation correction). The XRD refinement results indicate the model fitting the X-ray data as well. All refinement results and conditions were recorded into the corresponding Crystallographic Information Files (CIF), and these files are available from Supporting Information.

Results and Discussion

Crystal Structure of High Temperature Trigonal $ZrWMoO_8$ (HTT-$ZrWMoO_8$). The in situ XRD pattern of the HTT-$ZrWMoO_8$ phase at 750 °C is shown in Figure 1. The reflections were indexed in the trigonal crystal system with resulting cell parameters of a = 5.8355(1) Å and c = 6.0628(2) Å. The XRD pattern as well as the indices of the HTT-$ZrWMoO_8$ is similar to that of trigonal α′-$ZrMo_2O_8$. Given the isomorphism between $ZrMo_2O_8$ and ZrW_2O_8, the crystal structure of α′-$ZrMo_2O_8$ was chosen as the starting structure model to refine the crystal structure of HTT-$ZrWMoO_8$ by the Rietveld method, in which half the W atoms are substituted by Mo atoms. The refined XRD plot of HTT-$ZrWMoO_8$ and the final results are shown in Figure

(23) Kameswari, U.; Sleight, A. W.; Evans, J. S. O. *Int. J. Inorg. Mater.* **2000**, *2*, 333.
(24) Zhao, X.-h.; Huang, L.; Liu, P.-h.; Ma, H. *Chin. J. Chem.* **2003**, *21*, 1529.
(25) Dong, C. *J. Appl. Crystallogr.* **1999**, *32*, 838.
(26) Holland, T. J. B.; Redfern, S. A. T. *Mineral. Mag.* **1997**, *61*, 65.
(27) Larson, A. C.; Von Dreele, R. B. *General Structure Analysis System (GSAS)*; Los Alamos National Laboratory Report LAUR 86-748; Los Alamos National Laboratory: Los Alamos, NM, 2000.
(28) Toby, B. H. *J. Appl. Crystallogr.* **2001**, *34*, 210.
(29) Dilanian, R. A.; Izumi, F. *VIsualization of Crystal Structures - II*, Version 0.92.6; 2006.

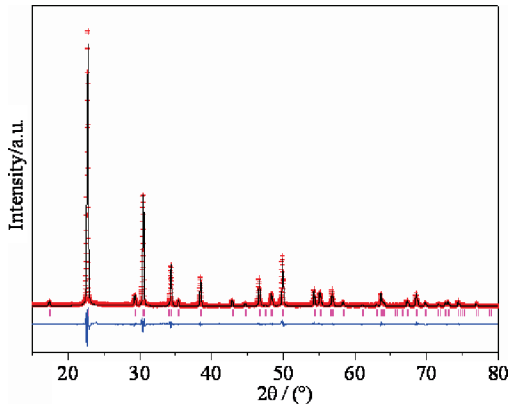

Figure 1. Final Rietveld refined XRD plot and difference plot for HTT-$ZrWMoO_8$. The crosses are the observed data, the solid line is the calculated pattern, and the tick marks indicate the calculated reflection positions. The difference curve is plotted below.

Table 1. Refinement Results for LTT-$ZrWMoO_8$[a] and HTT-$ZrWMoO_8$[b]

	LTT-$ZrWMoO_8$	HTT-$ZrWMoO_8$
space group	$R\bar{3}$	$P\bar{3}m1$
a (Å)	9.8722(1)	5.8404(1)
c (Å)	17.5455(2)	6.0671(2)
V (Å^3)	1480.905(20)	179.223(7)
R_{wp}	0.0534	0.083
R_p	0.0371	0.0588
R_F^2	0.03225	0.08807
R_e	0.0419	0.0280
goodness-of-fit, S	1.28	2.98

[a] The data obtained from X-ray refinement. [b] The data obtained from neutron refinement.

1 and Table 1, respectively. The polyhedral representations of the HTT-$ZrWMoO_8$ crystal structure are presented in Figure 2.

To compare with the structure of LTT-$ZrWMoO_8$, some features of the HTT-$ZrWMoO_8$ structure are emphasized here so that the HTT-$ZrWMoO_8$ structure can be described as a stacking of layers of corner-sharing ZrO_6 octahedra and MO_4 (M = W/Mo) tetrahedra. As shown in Figure 2 the layers parallel to (001) planes and the building period of layers are a single stack. The linkage between ZrO_6 and MO_4 coordination polyhedra in a stack is the same as that in the cubic ZrW_2O_8 crystal structure. The orientations of all ZrO_6 octahedra are identical, whereas MO_4 tetrahedra in a single stack, which is associated with an inversion center, point toward the ⟨001⟩ direction with $M-O_{terminal}$ bonds.

The distances between an $O_{terminal}$ atom and the closest Zr as well as M atom in the adjacent stack are 4.33 Å and 3.508 Å, respectively. The large interatomic distance indicates that only a weak Van der Waals force exists between stacks.

Crystal Structure of Low Temperature Trigonal $ZrWMoO_8$ (LTT-$ZrWMoO_8$). Figure 3 shows the XRD pattern of the LTT-$ZrWMoO_8$ sample. All peaks of the pattern can be indexed as trigonal symmetry without question. According to the extinction condition of the pattern the possible space groups are $R3$, $R\bar{3}$, $R32$, $R3m$, and $R\bar{3}m$. The cell parameters of LTT-$ZrWMoO_8$ (a = 9.8665(3) Å, c = 17.5330(89) Å) are similar to those of trigonal ZrW_2O_8 phase (a = 9.81 Å, c = 17.6 Å) with unknown crystal structure.[21] Wilkinson et al.[20] also synthesized a trigonal ZrW_2O_8 phase (a' = 9.81 Å, c' = 11.73 Å) using a nonhydrolytic sol–gel method; however, the parameter c' is shorter than the present parameter c, and the phase was identified as another isomorph of trigonal α-$ZrMo_2O_8$ (space group $P\bar{3}1c$).

It is clear from Figure 3 (insets a and b) that the indices of $hk0$ reflections remain identical in both LTT-$ZrWMoO_8$ and α-$ZrMo_2O_8$, but the $00l$ indices of the former are 3/2 times those of the latter. Because of the isomorphism between the two high temperature phases of HTT-$ZrWMoO_8$ and α′-$ZrMo_2O_8$ and the polytypism of α′-$ZrMo_2O_8$ and α-$ZrMo_2O_8$, considered together with the relationship between cell parameter values a(LTT-$ZrWMoO_8$) ≈ a(α-$ZrMo_2O_8$) and c(LTT-$ZrWMoO_8$) ≈ 1.5c (α-$ZrMo_2O_8$) (α-$ZrMo_2O_8$, a = 10.1416 Å, c = 11.7129 Å),[22] it is deduced that LTT-$ZrWMoO_8$ has a structure similar to that of α-$ZrMo_2O_8$, instead of a building period of stacking from two to three. The structure model gives rise to a formula number of 9 in a unit cell. This result coincides well with the measured crystal density of 5.1 g·cm^{-3}. The initial atomic positions (x, y, z) of the structural model are set with the atomic coordinates of α-$ZrMo_2O_8$ ($x = x'$; $y = y'$; $z = 2/3z'$, where x', y', z' are the atomic coordinates for α-$ZrMo_2O_8$), in which the coordinate z is adjusted to match the multiple unit vector c of LTT-$ZrWMoO_8$. Therefore, based on the above discussion, the structure of LTT-$ZrWMoO_8$ was solved and refined with the structure model by using Rietveld method. The refinement results and the refined NPD pattern of LTT-$ZrWMoO_8$ are shown in Table 1 and Figure 4, respectively. The refined XRD pattern and bond valence calculation results are available from Supporting Information.

Compared to the HTT-$ZrWMoO_8$ structure, the building period of layers of the LTT-$ZrWMoO_8$ structure changes to three stacks, as shown in Figure 5. The linkage between ZrO_6 octahedra and MO_4 tetrahedra remain identical within a stack as that of HTT-$ZrWMoO_8$, but the metal–oxygen polyhedron symmetry is lower than that of HTT-$ZrWMoO_8$ as a result of distortion of polyhedron (Table 2). In the LTT-$ZrWMoO_8$ structure, the Zr position splits into two types of point symmetry: Zr1 and Zr2. The octahedron of Zr1 with six O3 atoms is slightly distorted because the bond angle of O3−r1−O3 deviates slightly from 90°, although the bond length of six Zr1−O3 is equal. The six Zr2−O bonds of ZrO_6 octahedron separate into two groups: three Zr2−O1 and three Zr2−O2 bonds, and the values of distortion index D (bond length)[30] and bond angle variance σ^2 [31]are both larger than that in $Zr1O_6$ octahedron. As all bond lengths and bond angles of an MO_4 tetrahedron are different from each other, and the MO_4 tetrahedron is significantly distorted to an irregular polyhedron. It must be emphasized that the bond angle variance σ^2 of LTT-$ZrWMoO_8$ is especially large.

Bond valence calculations [32,33] for LTT-$ZrWMoO_8$ show that significant polyhedral distortion of MO_4 tetrahedron introduces extra $M\cdots O_{terminal}$ interaction (we call it secondary bonds) between the M atom and the closest neighboring terminal oxygen atom of the MO_4 tetrahedron between the adjacent stacks. The additional bond valence is 0.21.

(30) Baur, W. H. *Acta Crystallogr., Sect. B* **1974**, *30*, 1195.
(31) Robinson, K.; Gibbs, G. V.; Ribbe, P. H. *Science* **1971**, *172*, 567.
(32) Brown, I. D.; Shannon, R. D. *Acta Crystallogr., Sect. A* **1973**, *29*, 266.
(33) Brown, I. D.; Wu, K. K. *Acta Crystallogr., Sect. B* **1976**, *32*, 1957.

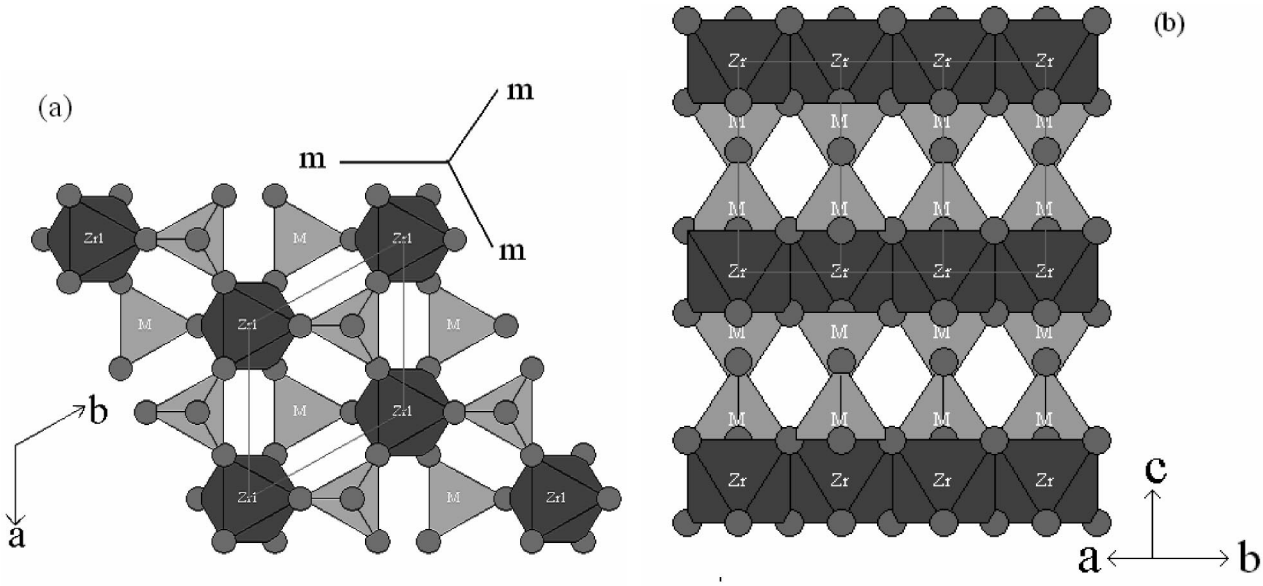

Figure 2. Polyhedral representations of the two-dimensional structural stack along [001] (a) and the close packing of stacks of HTT-$ZrWMoO_8$ along [210] (b). $\vec{a}$,$\vec{b}$,and $\vec{c}$ represent the translation vectors of the lattice, and *m* represents the mirror planes with respective directions.

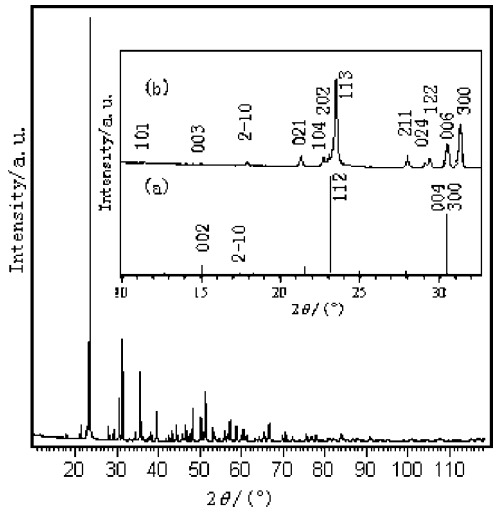

Figure 3. XRD pattern of LTT-$ZrWMoO_8$ at room temperature. The inset shows some of the reflections for α-$ZrMo_2O_8$ according to JCPDS (77-1784) (a) and LTT-$ZrWMoO_8$ (b). The indices are displayed near the reflections.

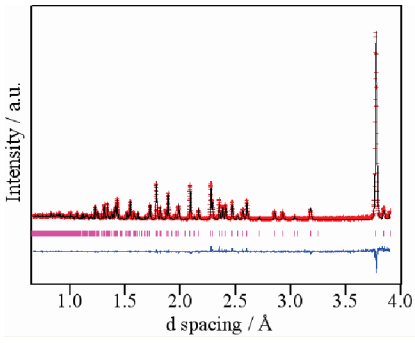

Figure 4. Final Rietveld refined NPD plot and difference plot for LTT-$ZrWMoO_8$. The crosses are the observed neutron diffraction data, the solid line is the calculated pattern, and the tick marks indicate the calculated reflection positions. The difference curve is plotted.

Consequently in the neighboring layer, terminal oxygen in MO_4 tilts toward the closest nearby MO_4, leading to a 23° angle between the M−O4 ($M-O_{terminal}$) bond direction and the [001] direction. The distance between this terminal oxygen and the next closest M atom in the nearby layer is only 2.46 Å, which is shorter than the interatomic distance of resulting from Van der Waals force as that in HTT-$ZrWMoO_8$. So the idea is reasonable that there is a secondary bond interaction adding to the existing Van der Waals force.

Significant polyhedral distortions in $Zr2O_6$ and MO_4also introduce corresponding distortion in every layer. Structure refinement results showed that Zr1 position was chosen as the origin of the unit cell, and Zr2 atoms have fractional coordinates (2/3, 1/3, 0.037) and (1/3, 2/3, −0.037), respectively. Thus, in the LTT-$ZrWMoO_8$ structure, the stacks form waggling layers instead of flat ones, as illustrated in Figure 5.

Both LTT-$ZrWMoO_8$ and α-$ZrMo_2O_8$ are polytype modifications of α′-$ZrMo_2O_8$ structure. The difference lies in the fact that the latter consists of two stacks as the repeating unit and the former contains three. The change of distortion parameters in metal–oxygen polyhedron between the two phases is comparable in value except for the bond angle variance σ^2 of MO_4 (Table 2). In LTT-$ZrWMoO_8$, half of the Mo atoms are substituted by W with weaker valence bonds, introducing larger bond angle distortion of MO_4 than that in α-$ZrMo_2O_8$. The emergence of secondary bonds in turn leads to folding or stacking in LTT-$ZrWMoO_8$ and gives rise to 3_1 symmetry compared with only glide plane symmetry existing in the α-$ZrMo_2O_8$ structure.

Phase Transition between LTT-$ZrWMoO_8$ and HTT-$ZrWMoO_8$. In situ temperature variable XRD experiments (Figure 6) indicate that LTT-$ZrWMoO_8$ transforms to HTT-$ZrWMoO_8$ when heated, and DSC analysis data (Figure 7) show that this phase transformation is reversible. The transition temperature is about 250 °C on the heating cycle, and the reversed phase transformation is about 212 °C on the cooling cycle as a result of thermal lag. The enthalpy change is small; therefore, the HTT-$ZrWMoO_8$ phase could not be obtained by the usual quenching method.

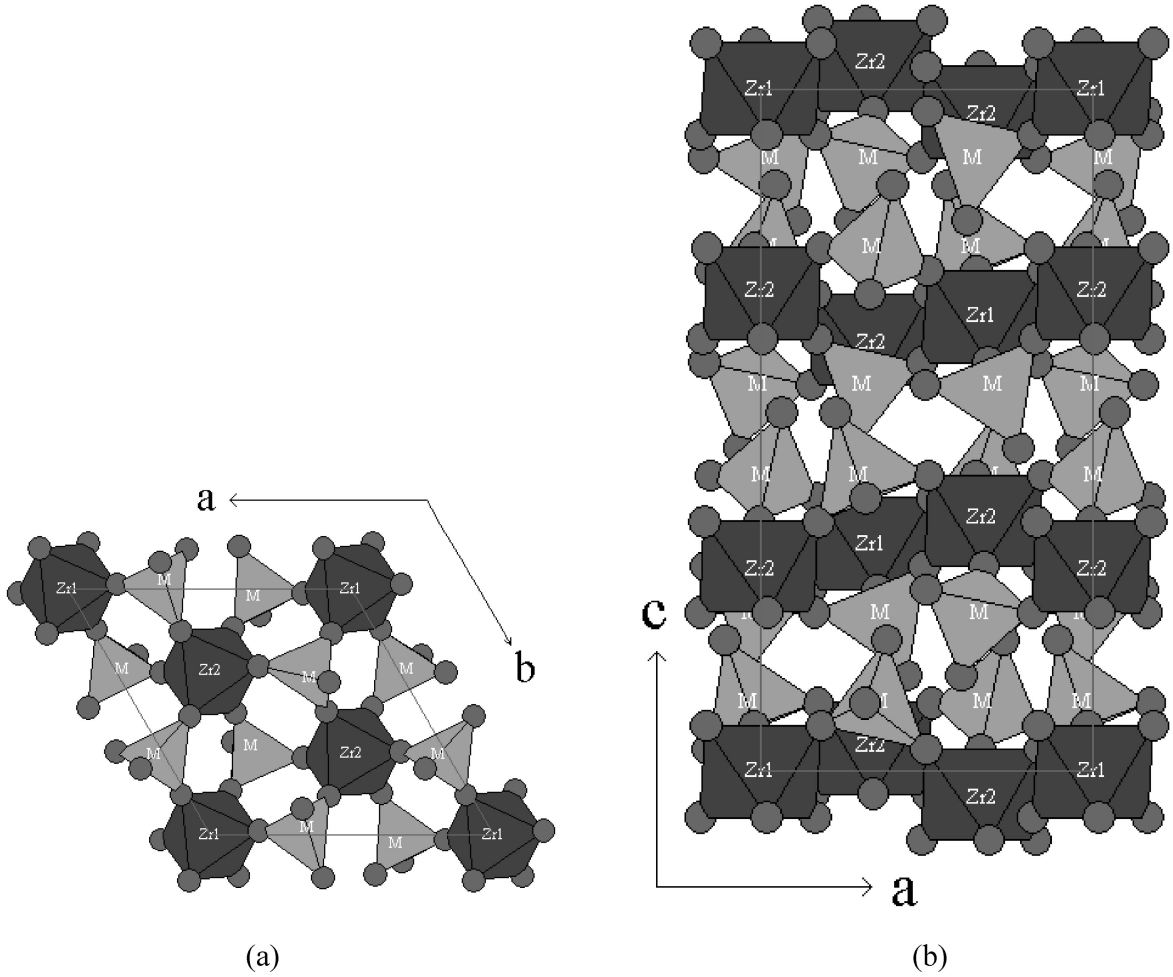

Figure 5. Polyhedral representations of the two-dimensional structural stack along [001] (a) and the close packing of stacks in LTT-ZrWMoO$_8$ along [010] (b). $\vec{a}$,$\vec{b}$,and $\vec{c}$ represent translation vectors of the lattice.

Table 2. Distortion Parameters[30,31] in Metal–Oxygen Coordination Polyhedra of HTT-ZrWMoO$_8$, LTT-ZrWMoO$_8$, and α-ZrMo$_2$O$_8$[a]

	HTT-ZrWMoO$_8$		LTT-ZrWMoO$_8$			α-ZrMo$_2$O$_8$		
	ZrO_6	MO_4	$Zr1O_6$	$Zr2O_6$	MO_4	$Zr1O_6$	$Zr2O_6$	MoO_4
distortion index (bond length)*D*	0.000	0.044	0.000	0.006	0.011	0.000	0.001	0.016
bond angle variance σ^2 (deg^2)	0.241	1.930	1.422	7.484	48.145	1.598	3.327	1.543

[a] The coordinates reported by Auray et al.[19] were used to calculate the distortion parameters.

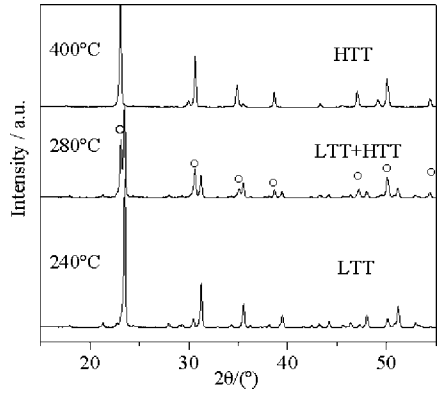

Figure 6. In situ XRD patterns of trigonal ZrWMoO$_8$ at different temperatures. Open circles indicate extra HTT-ZrWMoO$_8$ reflections at higher temperature.

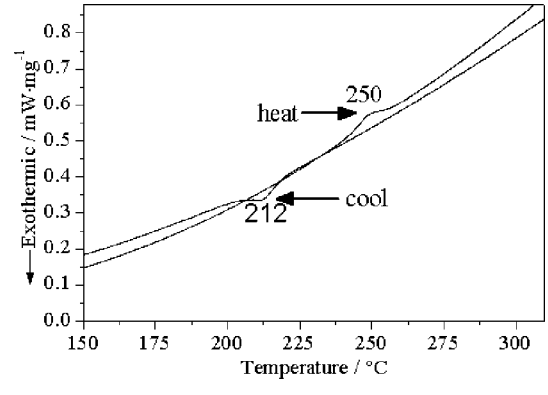

Figure 7. DSC curves of LTT-ZrWMoO$_8$ between 150 and 300 °C.

The cell parameter and volume changes of trigonal ZrWMoO$_8$ with temperature are plotted in Figure 8. For LTT-ZrWMoO$_8$ they all increase with temperature between 25 and 280 °C, the volume (α_V ($\times 10^{-6}$/°C) = $(V_{T_2} - V_{T_1})/(V_{T_1}(T_2 - T_1))$) and linear ($\alpha_l$ ($\times 10^{-6}$/°C) = $(l_{T_2} - l_{T_1})/(l_{T_1}(T_2 - T_1))$) thermal expansion coefficients are $\alpha_V = 70(2)$, $\alpha_a = 24.5(9)$, and $\alpha_c = 20(1)$, respectively. For HTT-ZrWMoO$_8$ cell volume and cell parameter *c* also increase with temper-

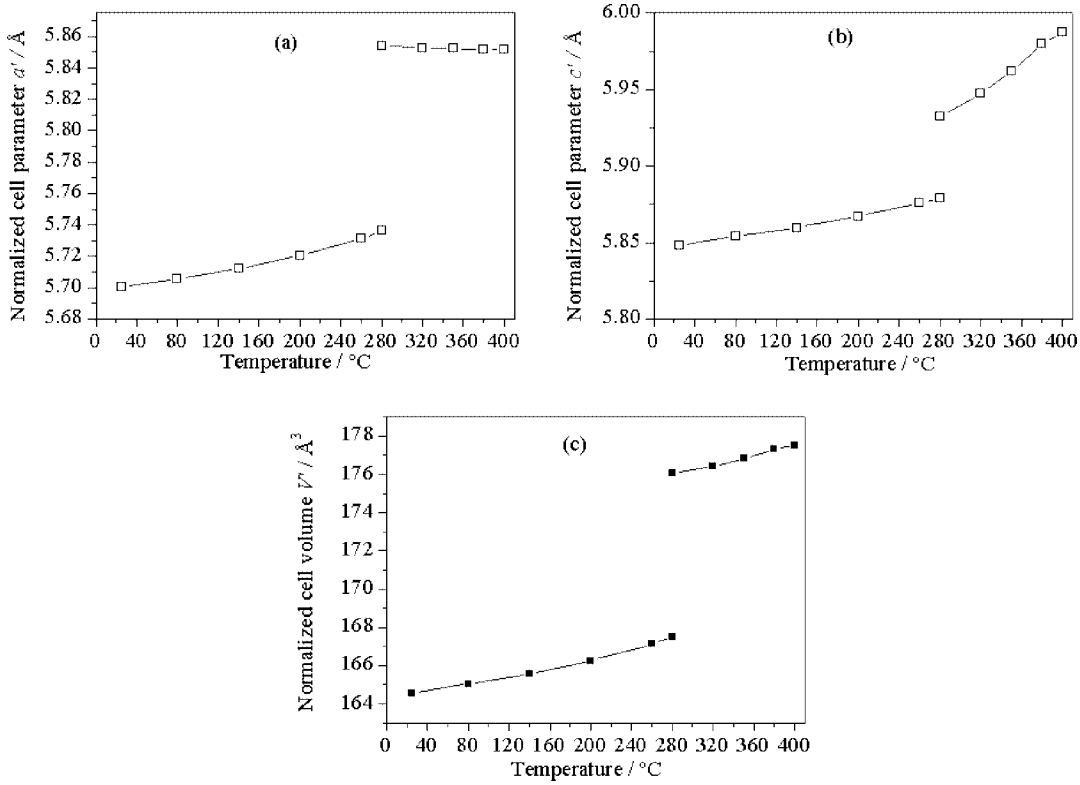

Figure 8. Temperature dependence of normalized cell parameters: a' (a), c' (b), and cell volume V' (c) for trigonal $ZrWMoO_8$. For convenience, the cell parameters and cell volume were normalized. The normalized cell parameter $a' = a/1.732$, $c' = c/3$ and cell volume $V' = V/9$ for LTT-$ZrWMoO_8$ and $a' = a$, $c' = c$, *and* $V' = V$ for HTT-$ZrWMoO_8$ (a, c, and V are cell parameters and cell volume, respectively).

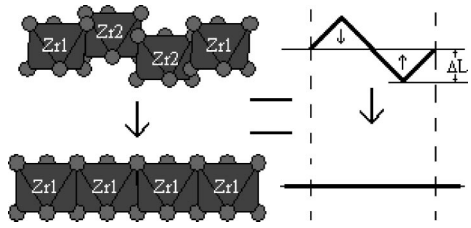

Figure 9. Illustration of which stack folding ΔL changes when LTT-$ZrWMoO_8$ transforms into HTT-$ZrWMoO_8$.

ature between 280 and 400 °C with $\alpha_V = 69(3)$ and $\alpha_c = 77(2)$, while the cell parameter a decreases with temperature with $\alpha_a = -4(1)$.

HTT-$ZrWMoO_8$ demonstrates NTE in two dimensions (*ab* plane) compared to that of isotropic NTE in cubic ZrW_2O_8. This is consistent with the fact that identical polyhedron corner sharing between ZrO_6 octahedron and MO_4 tetrahedron exists in the *ab* plane of the HTT-$ZrWMoO_8$ structure as in cubic ZrW_2O_8. The rigid unit modes (RUMs)[4,6] which were proposed to lead to NTE are expected to function similarly here, the difference being a 2-D case instead of 3-D.

The positive thermal expansion of LTT-$ZrWMoO_8$ in the *ab* plane is related to the folding ($\Delta L = 0.65$ Å) of stacks, as shown in Figure 9. When the temperature is raised, the degree of this folding ΔL gradually decreases, leading to the expansion of the stack dimension in the *ab* plane. This expansion overwhelms the lattice shrinking effect because of the rigid unit mode motions, giving rise to positive thermal expansion. This model is supported by the fact that the thermal expansion coefficients of cell parameter a decrease with stack folding ΔL in LTT-$ZrWMoO_8$, α-$ZrMo_2O_8$, and α′-$ZrMo_2O_8$ (HTT-$ZrWMoO_8$).

The large thermal expansion coefficients for cell parameter c in HTT-$ZrWMoO_8$ are due to the fact that the interaction between stacks along the c direction are van der Waals forces in nature, which also explains why the thermal expansion coefficient for cell parameter c is smaller in LTT-$ZrWMoO_8$, as an additional "secondary bond" is present in its structure compared with that of HTT-$ZrWMoO_8$.

The significant additional "secondary bond" present in LTT-$ZrWMoO_8$ is also the reason why the phase transformation to HTT-$ZrWMoO_8$ is a first order transition instead of a second order displacement phase transition, such as the one between α-$ZrMo_2O_8$ and α′-$ZrMo_2O_8$. This is strongly supported by experiment observations of a sudden increase of unit cell volume, thermal lag, and endothermic heat as shown in Figures 7 and 8.

Phase Transition between Cubic $ZrWMoO_8$ and Trigonal $ZrWMoO_8$. In Figure 10 the DSC curve of LTT-$ZrWMoO_8$ exhibits an endothermic peak around 921 °C. According to the in situ variable temperature XRD patterns as shown in Figure 11, the phase transition takes place at around 900 °C from HTT-$ZrWMoO_8$ to cubic $ZrWMoO_8$ structures. The XRD pattern of cubic $ZrWMoO_8$ at 25 °C synthesized by quenching is also shown in Figure 11. The indexed result indicates that it adopts the β-ZrW_2O_8 structure with cell parameter $a = 9.1377$ (1) Å, which is similar with the value 9.1400 (5) Å reported by Sleight et al.[23] During the sintering process, the weight loss of this sample which is attributed to the volatility of MoO_3 is 1.3 wt %, so the

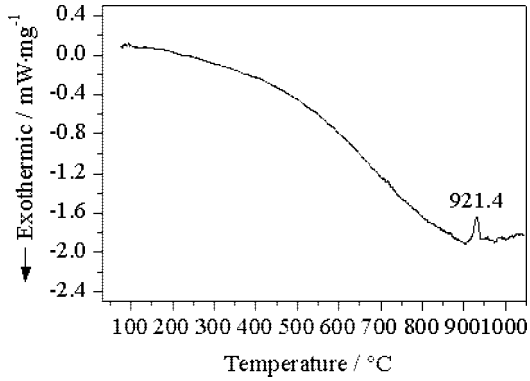

Figure 10. LTT-ZrWMoO$_8$ DSC scan, the slope comes from instrument background.

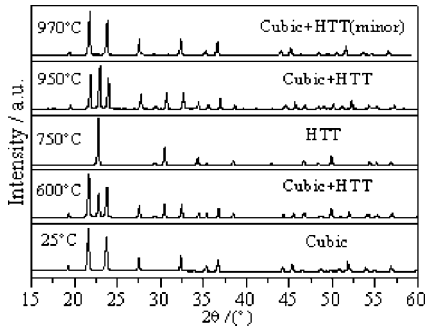

Figure 11. In situ variable temperature XRD patterns of cubic ZrWMoO$_8$ at different temperatures.

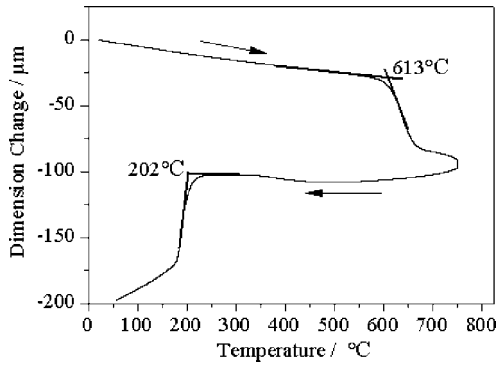

Figure 12. TMA curve of metastable cubic ZrWMoO$_8$.

exact formula is $ZrW_{1.02}Mo_{0.98}O_8$ accompanied with trace ZrO_2 in the material.

Figure 12 shows the result of TMA data for a cubic ZrWMoO$_8$ ceramic pellet sample under a circulatory heating process. The metastable cubic ZrWMoO$_8$ demonstrates excellent bulk NTE property below 600 °C. At 613 °C, the bulk length shrinks dramatically, corresponding to the phase transition from cubic ZrWMoO$_8$ to higher density HTT-ZrWMoO$_8$ according to variable temperature XRD patterns shown in Figure 11. The circulatory heating results indicate that the cubic phase is only metastable at room temperature. When the temperature decreases to 200 °C, the further decrease of bulk size corresponds to the transformation of HTT-ZrWMoO$_8$ to LTT-ZrWMoO$_8$ rather than cubic ZrWMoO$_8$.

Cubic ZrWMoO$_8$ is a 3-D framework structure while HTT-ZrWMoO$_8$ is a layered structure, the phase transition in between involves reconstruction of chemical bonds and is therefore a reversible first order reconstructive phase transition. The transformation is slow with obvious volume change and latent heat.

From the results above, the phase transformation relationship among LTT-, HTT-, and cubic-ZrWMoO$_8$ is thus established as showing in eq 1:

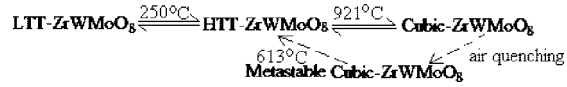

(1)

The phase transformation relationship between the stable cubic phase, trigonal phases, and metastable cubic phase for ZrWMoO$_8$ is different from the known phase transition in the $ZrW_{2-x}Mo_xO_8$ solid solution system. When $x = 0$, metastable cubic ZrW_2O_8 decomposes into corresponding oxides, and with heating to 773 °C, no trigonal ZrW_2O_8 phase emerges.[12] The trigonal phase was only separately synthesized by the nonaqueous sol–gel method.[20,21] When $x = 2$, cubic $ZrMo_2O_8$ can be prepared through dehydration of the $ZrMo_2O_7(OH)_2 \cdot 2H_2O$ precursor within a very narrow temperature window by inhibiting the formation of the trigonal phase.[2,18,34] Although the metastable cubic $ZrW_{2-x}Mo_xO_8$ phases can transform to trigonal phases at high temperature when the W/Mo ratio is smaller than 1, there are no reports that the trigonal phase can transform to the cubic phase directly. Before now, no trigonal phases were reported in $ZrW_{2-x}Mo_xO_8$ solid solutions when $x \leq 1$. In this study, when $x = 1$, reversible phase transition occurs among trigonal and cubic ZrWMoO$_8$ phases. Therefore, it is reasonable to predict that thermodynamic equilibrium can be reached between trigonal and cubic $ZrW_{2-x}Mo_xO_8$ phases within a certain composition range around $x = 1$ and cubic phases of $ZrW_{2-x}Mo_xO_8$ could be synthesized through polymorphous transformation.

Compared to direct high temperature solid state reaction or precursor dehydration route, synthesis of $ZrW_{2-x}Mo_xO_8$ solid solutions through polymorphous transformations is easier. It is also possible to prepare single component composite material involving cubic and trigonal phases with an adjustable thermal expansion coefficient utilizing the $ZrW_{2-x}Mo_xO_8$ solid solution phase transformation and equilibrium properties.

Conclusion

Two new phases of ZrWMoO$_8$, HTT-ZrWMoO$_8$ and LTT-ZrWMoO$_8$, were found in this study. The HTT-ZrWMoO$_8$ is isomorphous with α′-$ZrMo_2O_8$ with symmetry of space group $P\bar{3}m1$, and the cell parameters are $a = 5.8404(1)$ Å and $c = 6.0671(2)$ Å. The LTT-ZrWMoO$_8$ crystal structure is similar to that of α-$ZrMo_2O_8$, being two different polytypes of the α′-$ZrMo_2O_8$ structure. On the basis of this model, the LTT-ZrWMoO$_8$ crystal structure was successfully solved and refined in space group $R\bar{3}$, and the cell parameters are $a = 9.8722(1)$ Å and $c = 17.5455(2)$ Å. Because Mo atoms are partially substituted by W, there is larger coordination polyhedron distortion, more significant structural layer fold-

(34) Lind, C.; Wilkinson, A. P.; Rawn, C. J.; Payzant, E. A. *J. Mater. Chem.* **2001**, *11*, 3354.

ing, and additional $M\cdots O_{terminal}$ interaction between structure blocks in LTT-$ZrWMoO_8$ compared with those in α-$ZrMo_2O_8$. These differences between the two structures were also shown to correlate consistently with the observed different thermal expansion properties. The phase transitions between two trigonal forms and between HTT-$ZrWMoO_8$ and the cubic forms are reversible first order phase transitions. The results reveal that a certain composition range exists around a 1:1 W to Mo ratio, where cubic $ZrW_{2-x}Mo_xO_8$ and single composition cubic and trigonal composite material with adjustable thermal expansion coefficient could be prepared utilizing the polymorphous phase transitions existing in the system.

Acknowledgment. Project 20471010 supported by National Natural Science Foundation of China and the Foundation of Beijing Key Discipline of Inorganic Chemistry of Beijing Education Committee are gratefully acknowledged. Argonne National Laboratory's work was supported by the U.S. Department of Energy, Office of Science, Office of Basic Energy Sciences, under Contract No. DE-AC02-06CH11357.

Supporting Information Available: The Crystallographic Information Files (CIF) of HTT-$ZrWMoO_8$ and LTT-$ZrWMoO_8$ and the refined XRD pattern and the bond valence calculation results of LTT-$ZrWMoO_8$ (PDF). This material is available free of charge via the Internet at http://pubs.acs.org.

CM071605Y